Determination of the minority carrier diffusion length in compositionally graded $Cu(In,Ga)Se_2$ solar cells using electron beam induced current

Gregory Brown,[1,a)] Vladimir Faifer,[1] Alex Pudov,[1] Sergey Anikeev,[1] Eugene Bykov,[1] Miguel Contreras,[2] and Junqiao Wu[3,4]
[1]*Nanosolar, Inc, San Jose, California 95138, USA*
[2]*National Renewable Energy Laboratory, Golden, Colorado 80401, USA*
[3]*Department of Materials Science and Engineering, University of California, Berkeley, California 94720, USA*
[4]*Division of Materials Sciences, Lawrence Berkeley National Laboratory, Berkeley, California 94720, USA*

(Received 28 October 2009; accepted 15 December 2009; published online 14 January 2010)

A method is proposed and tested which allows for the accurate determination of the carrier collection efficiency and minority carrier diffusion length in $Cu(In,Ga)Se_2$ solar cells using energy dependent electron beam induced current. Gallium composition gradients across the film thickness introduce quasielectric fields that are found to improve collection efficiency when they are located toward the rear of the sample. The quasielectric fields are also shown to reduce the influence of back surface recombination. The strengths and limitations of this technique are discussed and compared with external quantum efficiency measurements. © *2010 American Institute of Physics*.
[doi:10.1063/1.3291046]

$Cu(In,Ga)Se_2$ (CIGS) solar cells have achieved efficiencies above 19% using a compositionally graded profile.[1] Despite this, it is still very difficult to measure many of the fundamental parameters of CIGS such as the bulk minority carrier diffusion length, which should strongly influence overall device performance. In order to further improve upon device efficiencies, it is necessary to understand how the specific properties of CIGS affect the overall device performance.

One of the most widely used techniques to understand minority carrier properties in CIGS is time resolved photoluminescence (TRPL).[2] However, while some studies have shown minority carrier lifetime influences device performance,[3] others have found no correlation.[4] One reason for this discrepancy is that TRPL studies on CIGS are very sensitive to exposure to air, incident photon flux and whether the measurement is performed on a completed junction.[5]

Electron beam induced current (EBIC) can also be used to measure the bulk minority carrier diffusion length.[6] This approach has previously been used to measure the diffusion length in compositionally uniform $Cu(In,Ga)(Se,S)_2$ films.[7–9] However, the best CIGS solar cells have a compositionally graded profile.[10] The graded profile results in a quasielectric field which improves minority carrier collection and must be considered to give an accurate estimate of the bulk diffusion length.[11] Therefore, it is imperative to develop a reliable technique that can quantitatively measure the minority carrier diffusion length in compositionally graded CIGS solar cells.

Energy dependent EBIC measurements were collected in the planar configuration for CIGS solar cells with different composition profiles as shown in Fig. 1(a). The four cells discussed in this letter were grown by vacuum coevaporation at the National Renewable Energy Laboratory. The EBIC measurements were performed on a Hitachi SU-1500 scanning electron microscope at beam energies between 2 and 30 kV. The EBIC and beam current were measured using a current preamplifier (Stanford Research Systems SR570). The electron beam was defocused and kept constant at 100 pA, as measured by a faraday cup mounted on the specimen holder. The electron beam impacted an area of roughly 0.025 mm^2.

High frequency (100 kHz) capacitance measurements were also performed on each sample at −170 °C to determine the space charge width. The low temperature and high frequency was required to avoid the capacitance contribution from surface defects and deep levels within the bulk. The Gallium composition profiles were determined by secondary ion mass spectroscopy and are shown in Fig. 1(b). One

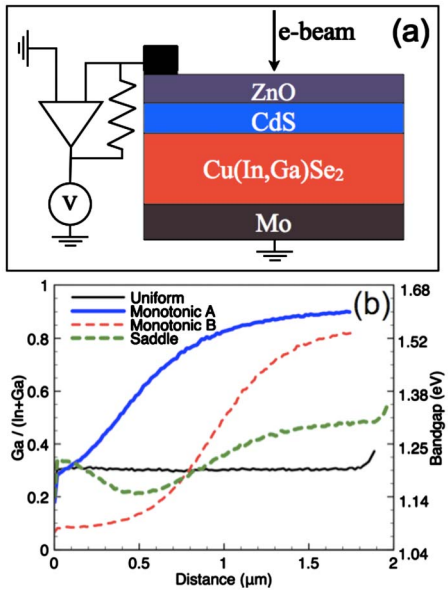

FIG. 1. (Color online) (a) The device structure and geometry used in the EBIC measurements. (b) Gallium alloy fraction and corresponding band gap as a function of depth obtained by secondary ion mass spectroscopy.

[a)]Electronic mail: gregory.brown@nanosolar.com.

TABLE I. Solar simulator results showing the operating characteristics of the four devices. The space charge width (SCR) is obtained by the low temperature capacitance of each sample. The minority carrier diffusion length (L) is obtained by the EBIC quantum efficiency versus beam voltage.

Sample	J_{sc} (mA/cm^2)	V_{oc} (mV)	Fill Factor	η	SCR (μm)	L (μm)
Uniform	30.44	656.2	0.769	15.36	0.42	>0.91
Monotonic A	27.97	736.9	0.741	15.27	0.56	0.30
Monotonic B	34.28	666.3	0.752	17.17	0.70	0.35
Saddle	32.16	668.2	0.790	16.97	1.18	0.52

sample has a uniform Ga concentration, two samples have roughly linearly increasing Ga concentrations (monotonic A and B) and the final sample has a saddle shaped profile which is standard for the highest efficiency NREL cells.[10]

Table I shows the device parameters, space charge width and minority carrier diffusion length determined by energy dependent EBIC. First, the measured EBIC was divided by the total number of electron-hole pairs (EHPs) generated in the film to obtain a quantum efficiency. The depth distribution of the electron energy dissipation function was used to calculate the EHP generation rate. This function can be described by a modified Gaussian as discussed in Ref. 6. Monte Carlo simulations were also performed to ensure the validity of the modified Gaussian function for the device structure. Four separate layers were considered as follows: 200 nm of ZnO, 80 nm of CdS, 2000 nm of CIGS, and the substrate. The thickness of the ZnO (CdS) layer was modified in the calculation by the ratio of ZnO (CdS) density to CIGS density. For simplicity, the density of the CIGS layer was assumed to be constant and equal to 5.57 g/cm^3. The arbitrary constants in the modified Gaussian distribution were determined by numerically integrating the depth dependent distribution and normalizing it to the incident electron beam power

$$G_0(\mathrm{cm}^{-2}\ \mathrm{sec}^{-1}) = 6.25 \times 10^{21} V j_b (1-k), \tag{1}$$

where V is the beam voltage in kV, j_b is the beam current in A/cm^2, and k is the fraction of backscattered electrons [assumed to be a constant value of 0.32 (Ref. 12)]. The depth dependent carrier generation rate $[g(V,z)]$ was then obtained by dividing the energy dissipation function by the mean energy required to make an EHP at each depth. The energy to make an EHP was also taken from Ref. 6

$$\xi = 2.596 E_g + 0.714, \tag{2}$$

where E_g is the band gap at each position. The band gap of ZnO (CdS) is 3.3 (2.42) and the compositionally dependent band gap for the CIGS layer is as follows[13]

$$E_g(\mathrm{CuIn}_{1-x}\mathrm{Ga}_x\mathrm{Se}_2) = 1.04(1-x) + 1.68x - 0.21x(1-x). \tag{3}$$

The measured quantum efficiency was simulated by numerically evaluating the integral[7,14]

$$e(V) = \eta \int_0^\infty F(z) g(V,z) dz, \tag{4}$$

where F is the carrier collection probability as a function of distance, g is the depth dependent carrier generation rate and η is a constant factor correcting for the shunt resistance of the cell. The shunt correction factor is necessary given the input impedance on the current preamplifier can approach the shunt resistance of the cell.

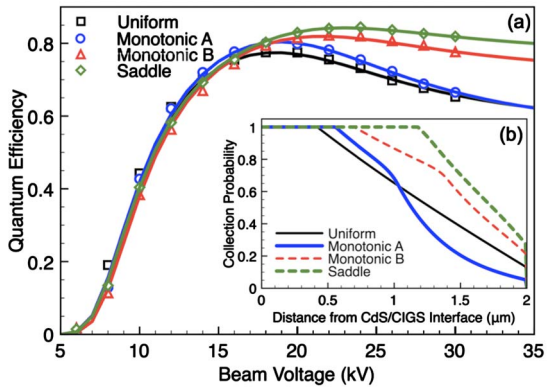

FIG. 2. (Color online) (a) EBIC quantum efficiency plots vs electron beam voltage. Solid curves are the result of theoretical calculations. Experimental points are displayed as symbols. The high voltage slope is used to calculate the bulk diffusion length. (b) Simulated collection probability vs distance used to obtain the solid curves in (a).

A constant carrier collection probability of 0 (0.2) was assumed for the ZnO (CdS) layers and all carriers generated within the space charge region are assumed to be collected. The carrier collection probability within the bulk neutral region was calculated assuming a constant minority carrier diffusion length, electron mobility and back surface recombination velocity. The diffusion length was allowed to vary from sample to sample while the electron mobility was fixed at 100 cm^2/Vsec (Ref. 15) and the back surface recombination velocity was fixed at 10^5 cm/sec. Three of the devices in this paper feature Gallium gradients throughout the bulk which establish a quasielectric field that aids minority carrier collection.[16] This effect was incorporated by dividing the CIGS layer into three distinct regions with an approximately constant electric field. The analytic equations presented in Ref. 16 were then used to calculate the collection probability within each region as a function of both the local electric field and bulk diffusion length. The collection probability as a function of distance through the CIGS layer was then determined by applying the appropriate boundary condition between each region.[16] The measured and simulated quantum efficiency curves as well as the simulated collection probability as a function of distance are shown in Fig. 2.

The EBIC quantum efficiency curves in Fig. 2(a) show measurable differences between the four cells even though all four exhibit high efficiencies (over 15%). The two highest efficiency cells with monotonic B and saddle profiles exhibited the highest quantum efficiencies with the least falloff at high beam voltage. The falloff at high beam voltage is most strongly dependent on the composition gradient and minority carrier diffusion length. This effect is most easily seen in Fig. 2(b) where the collection probability remains high toward the back of the sample. The monotonic A sample also features a large composition gradient, but most of it is located toward the front of the sample thereby reducing its benefit. The uniform sample suffers from a reduced collection probability due to the lack of a composition gradient.

The minority carrier diffusion length used to simulate the quantum efficiency plots is shown in Table I. The two samples with the largest gradients have diffusion lengths of 0.3 and 0.35 μm while the saddle shaped sample has a dif-

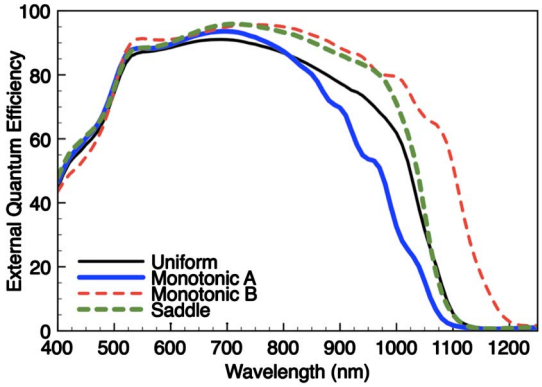

FIG. 3. (Color online) External quantum efficiency of each device vs wavelength. The observed long wavelength falloff in external quantum efficiency is consistent with the simulated collection efficiency in Fig. 2(b).

fusion length of 0.52 μm. It should be noted that the measured diffusion length can change among different samples with the same composition profile. 12 different samples with saddle shaped profiles were also measured and found to have diffusion lengths ranging from 0.5 to over 2 μm. The uniform sample has a diffusion length on the order of the film thickness, such that its collection probability function is primarily determined by the back surface recombination velocity. Previous experiments have suggested an extremely high back surface recombination velocity to carrier diffusivity ratio ($S_{Mo}/D_e \geq 10^7$).[17] However, our experimentally measured collection efficiency for the uniform sample sets an upper limit of 4×10^4 cm^{-1} for the S_{Mo}/D_e ratio.

Energy dependent EBIC is an accurate method to determine small diffusion lengths. However, it is less reliable when the diffusion length is on the order of the film thickness as it is necessary to assume a S_{Mo}/D_e ratio. This is most pronounced for the uniform sample where the diffusion length can range from 0.91 μm to the film thickness depending on which S_{Mo}/D_e ratio is used. On the other hand, the choice of S_{Mo}/D_e ratio has no effect on the monotonic samples due to their lower diffusion lengths and compositional grading. It should be noted that other techniques used to determine carrier diffusion lengths via collection efficiency (such as external quantum efficiency) have the same limitations. It was found that errors in the measured ZnO thickness and space charge width have the most influence on the EBIC fitting. For the monotonic A sample, a 10% error in the measured ZnO thickness or space charge width would change the diffusion length by roughly 6%. All other assumptions (carrier mobility, CdS collection efficiency, etc.) used to fit the monotonic A sample were found to affect the diffusion length by less that 1%. However, as the back surface gradient is diminished, these assumptions have a larger influence on the EBIC fitting due to the increasing effect of the back surface.

External quantum efficiency (EQE) measurements were collected for each cell and are shown in Fig. 3. A comparison between Figs. 2(b) and 3 highlights the dependence of EQE measurements on the composition profile within each sample. At long wavelengths, the light penetration depth is highly dependent on the band gap profile making it difficult to determine which sample has the highest collection efficiency. It is easier to estimate the electron beam penetration depth as it depends most strongly on material density which does not vary appreciably between $CuInSe_2$ and $CuGaSe_2$. The local bandgap only affects the measurement through a linear change in the energy required to make an EHP [Eq. (2)]. Although EQE can only be used qualitatively to determine collection efficiency, a comparison between Figs. 2(b) and 3 shows that samples with good carrier collection measured with EBIC also have high EQE.

In summary, energy dependent EBIC measurements were performed on CIGS solar cells with different Gallium profiles. This technique was used to determine the depth dependent collection probability and minority carrier diffusion length of each cell. The measurements provide evidence that the existence of quasielectric fields due to compositional grading are beneficial for improving carrier collection and reducing the impact of back surface recombination. EQE measurements were used to verify the accuracy of the technique.

We would like to thank the characterization team at Nanosolar, Inc. for helping with the measurements in this work, M. Contreras for providing the samples and J. Wu for a critical reading of the manuscript.

[1] I. Repins, M. A. Contreras, B. Egaas, C. DeHart, J. Scharft, C. Perkins, B. To, and R. Noufi, Prog. Photovoltaics **16**, 235 (2008).
[2] W. K. Metzger, I. L. Repins, and M. A. Contreras, Appl. Phys. Lett. **93**, 022110 (2008).
[3] B. Ohnesorge, R. Weigand, G. Bacher, A. Forchel, W. Riedl, and F. H. Karg, Appl. Phys. Lett. **73**, 1224 (1998).
[4] I. L. Repins, B. J. Stanbery, D. L. Young, S. S. Li, W. K. Metzger, C. L. Perkins, W. N. Shafarman, M. E. Beck, L. Chen, V. K. Kapur, D. Tarrant, M. D. Gonzalez, D. G. Jensen, T. J. Anderson, X. Wang, L. L. Kerr, B. Keyes, S. Asher, A. Delahoy, and B. Von Roedern, Prog. Photovoltaics **14**, 25 (2006).
[5] W. K. Metzger, I. L. Repins, M. Romero, P. Dippo, M. Contreras, R. Noufi, and D. Levi, Thin Solid Films **517**, 2360 (2009).
[6] C. J. Wu and D. B. Wittry, J. Appl. Phys. **49**, 2827 (1978).
[7] R. Scheer, C. Knieper, and L. Stolt, Appl. Phys. Lett. **67**, 3007 (1995).
[8] R. Scheer, M. Wilhelm, H. J. Lewerenz, H. W. Schock, and L. Stolt, Sol. Energy Mater. Sol. Cells **49**, 299 (1997).
[9] B. Sieber, C. M. Ruiz, and V. Bermudez, Superlattices Microstruct. **45**, 161 (2009).
[10] K. Ramanathan, M. A. Contreras, C. L. Perkins, S. Asher, F. S. Hasoon, J. Keane, D. Young, M. Romero, W. Metzger, R. Noufi, J. Ward, and A. Duda, Prog. Photovoltaics **11**, 225 (2003).
[11] A. M. Gabor, J. R. Tuttle, A. Schwartzlander, A. Tennant, M. A. Contreras, and R. Noufi, *Proceedings of the First World Conference on Photovoltaic Energy Conversion* (IEEE, New York, 1994) p. 83.
[12] R. Scheer, Philos. Mag. B **72**, 75 (1995).
[13] S. Wei and A. Zunger, J. Appl. Phys. **78**, 3846 (1995).
[14] C. Donolato, Appl. Phys. Lett. **46**, 270 (1985).
[15] M. Gloeckler, A. L. Fahrenbruch, and J. R. Sites, Proceedings of the Third World Conference on Photovoltaic Energy Conversion, Japan, 2003 (unpublished) pp. 491–494.
[16] M. A. Green, Prog. Photovoltaics **17**, 57 (2009).
[17] J. Mattheis, P. J. Rostan, U. Rau, and J. H. Werner, Sol. Energy Mater. Sol. Cells **91**, 689 (2007).